Gravimetric Detection of Cave Space and Sinkhole Hazard with Growth Inversion: Valaská Village Case in Karst (Slovakia)

Jozef Bódi , Peter Vajda * , Pavol Zahorec , René Putiška , Juraj Papčo , Roman Pašteka , José Fernández

Posted Date: 27 March 2026

doi: 10.20944/preprints202603.2217.v1

Keywords: near surface geophysics; 3D microgravimetry; inverse problem; growing source bodies; karst caverns; sinkhole hazard

Article

Gravimetric Detection of Cave Space and Sinkhole Hazard with Growth Inversion: Valaská Village Case in Karst (Slovakia)

Jozef Bódi [1,2,3], Peter Vajda [2,*], Pavol Zahorec [2], René Putiška [3], Juraj Papčo [4], Roman Pašteka [3] and José Fernández [1]

[1] Institute of Geosciences (IGEO), CSIC-UCM, Madrid, Spain
[2] Earth Science Institute, Slovak Academy of Sciences, Bratislava, Slovakia
[3] Dept. Engineering Geology, Hydrogeology and Applied Geophysics, Comenius University in Bratislava, Slovakia
[4] Dept. Global Geodesy and Geoinformatics, Slovak University of Technology, Bratislava, Slovakia
* Correspondence: peter.vajda@savba.sk

Abstract

Underground water flow in karst areas and changing water levels due to extreme rain can lead to creation of caverns and sinkhole hazard. Such is the historical experience of the Valaská village in central Slovakia. To better understand the current sinkhole threat in the village, we aim at detecting shallow caverns using microgravimetry. Our broader objective is to examine the capabilities of the Growth inversion methodology to detect and characterize shallow cave space. In our study we focus on the benefits and weak points of the Growth inversion approach, which is a free-geometry inversion method based on model exploration and growing source bodies. Since a sole gravimetric inversion produces ambiguous results, we pay attention to the role and setup of the several free user-adjustable inversion parameters of Growth. We examine tuning these parameters for specific needs of shallow cavities detection. Valaská experienced sinkholes in 1964, 1968 and 2019. That of 1964 is known for a curious loss of a horse sunk into a karst chimney. Our gravimetric work shows that the sinkhole hazard at the exposed lot in Valaská is ongoing despite the taken mitigation construction measures. The Growth approach proved to be applicable and useful in microgravimetric identification of sinkhole threat and detection of shallow caverns in karst.

Keywords: near surface geophysics; 3D microgravimetry; inverse problem; growing source bodies; karst caverns; sinkhole hazard

1. Introduction

Shallow void spaces, such as caverns in karst or mining galleries, can pose threat in terms of sinkhole development. It is important to detect the position, size and shape of such cavities to eliminate or mitigate the sinkhole hazard, particularly in urban areas. Several near-surface geophysical methods can be deployed to detect shallow cavities. One of them is microgravimetry. The density contrast of void (air-filled) or water-filled space relative to the surrounding rock or soil environment is strong enough to produce pronounced detectable lows in the gravity data, which can serve the identification and specification of the hidden underground cavities.

Microgravimetry has long been used to detect cavities in shallow subsurface and also specifically in karst areas (e.g., [1–8]). Electrical resistivity tomography (ERT) or imaging (e.g., [5,6,8–13]), ground penetrating radar (GPR) (e.g., [9]), seismic refraction tomography or seismic reflection (e.g., [10,14]) and other geophysical methods (e.g., [4,6,15,16]) have been also applied for detection of sinkholes or cave space.

 doi:10.20944/preprints202603.2217.v1

The gravity data for such purpose are collected with a high resolution at the level of 1 m. By high resolution we mean either irregularly spaced observation points with average spacing at the level of 1 m, or a regular rectangular grid of observation points with spacing at the level of 1 m. The data are observed with relative gravimeters at the highest achievable accuracy. When using the present-day gravimeters, indoors or in the field under calm conditions (no strong winds, no strong anthropogenic noise), accuracy at the level of 5 μGal (1 μGal = 10^{-8} m/s^2) is achievable. The data accuracy (and resolution) worked with gives rise to the name of this branch of gravimetry, namely microgravimetry.

The gravity data are typically observed on the topographic surface. Consequently, they are strongly affected by the gravitational effect of the terrain (topographic masses), especially in areas of rugged surface relief. In searching for subsurface cavities, this effect is unwanted, as it masks the gravitational effect of the cavities. The effect of topographic masses is therefore removed from the observed data. This correction is computed in the neighborhood of the studied area covered by data points, i.e., to a certain radial distance from each data point (typically 167 km). Sophisticated numerical methods exist for computing this correction. We use here a specific implementation in the form of Toposk software [17]. The observed gravity data corrected for the effect of topographic masses are referred to as the "complete Bouguer anomalies" abbreviated as "CBA data".

The CBA data can be affected by deeper density contrast boundaries, which produce gravitational effect that is in the context of the search for shallow cavities unwanted. This effect can be removed by correcting the CBA data for a computed regional, usually planar, trend. The "detrended" CBA data are often referred to as "residual CBA data" or simply "residual Bouguer anomalies" (RBA data). Occasionally, the RBA data are called "local Bouguer anomaly" (LBA). The RBA data represent the signal (gravitational effect) of local shallow subsurface density distribution. If cavities (void space) are present in the shallow subsurface, then the RBA field (map) is dominated by gravity lows of the cavities, because they represent the strongest density contrast of the shallow subsurface.

The remaining task is to translate the gravity lows of the RBA map into a 3D model of the subsurface cavities. This task involves solving the inverse gravimetric problem. Various approaches, methods and techniques exist to accomplish this task. We shall not give a comprehensive review of them here. Instead, we shall focus on just one of them, which is based on partitioning the subsurface into a set of layered right-rectangular prisms (cells) with sizes adequately related to the resolution of the gravity data on the surface, and iterative exploration and filling of those cells by a preselected density contrast (both positive and negative).

Throughout the iterative inversion process the aggregations of filled cells form growing source bodies. The process ends when the gravitational effect of the model source bodies reaches an adequate fit to the observed gravity data. Actually, the data fit is not the only condition in this iterative least-squares adjustment (LSA) inversion procedure. The data fit is complemented by forcing the solution (the "Growth model" as the result of the growth process) to be compact, which is a specific form of regularizing the inverse problem. Forcing the solution towards compact is achieved by minimizing the total mass of (both the positive and the negative contrast) source bodies. The balance between minimizing the data misfit and minimizing the total mass is controlled by the so-called balance factor, which provides weighting between the two minimizations throughout the iterative inversion process.

This inversion process, called "Growth", was developed by Camacho [18]. Originally it served for inverting CBA data in crustal structural studies. It was improved and upgraded in the GROWTH-2 [19,20], GROWTH-3 [21] and GROWTH-23 [22] implementations. A special version of Growth inversion, GROWTH-dg [23], was designed for specific needs of volcano gravimetry that typically faces sparse, low in number, scattered 4D microgravity data (spatiotemporal gravity changes) with low signal-to-noise ratio, observed in volcanic areas and usually associated with volcanic unrest (e.g., [24]. A particular version of the Growth inversion, operating with a cloud of spheres, possibly partly overlapping, had been applied to detect cave space in karst [25]. A comprehensive review of the Growth inversion approach, its historical developments and applicability across diverse earth science

 doi:10.20944/preprints202603.2217.v1

disciplines was given recently in [26]. The capabilities of Growth inversion to sinkhole hazard identification in undermined or urban areas was investigated also in [27,28]. Here we use the GROWTH-dg implementation of the inversion approach, as described in Section 3.

2. Sinkhole Hazard in Karst Area—Village of Valaská (Slovakia)

The village Valaská near the town Brezno in the Hron river valley of central Slovakia (see Figure 1 and the Supplementary Materials for its geographical location) is prone to sinkhole hazard due to underground watercourse in karst. Surface subsidence and small sinkholes had been observed by the inhabitants of Valaská around the Tajch spring since time immemorial. In 1964 a sinkhole accident occurred (see the Supplementary Materials). Farmer Michal Havrila returned on the evening of 21 September from the field and stalled his horse in the barn. Subsequently, the horse suddenly sank into a 9 m deep hollow [29]. Next day the horse was pulled up by the speleologist rescue, yet dead. The speleologists explored the sinkhole cavern. At the bottom of the 9 m deep cavern a debris cone of clay and rock was found. The slanted bottom entered a water pool 3 m deep. This cavern (hall) was interconnected with a neighboring one also containing a water pool. As revealed by later exploration, these caverns are part of a larger cave system. None of the halls had a limestone ceiling (see the cross-section in the Supplementary Materials, Figure S5). The ceiling was of solidified gravel and clay of the Hron river bench. The cavern spaces were created by elevated underground water levels and tend to attain shapes of karstic chimneys.

According to Putiška [30], engineering-geological and hydrogeological exploration of the subsurface of Valaská was carried out with assistance of speleologists and scuba-divers in 1965 [31]. In 1972 the to-date knowledge of the site was summarized by Kubíny [32]. It was concluded that the to-date knowledge had confirmed large-scale high-degree karstification of the Valaská underground in the forefront of the Tajch spring and the existence of deep extensive underground water pools. During anomalously high rainfall or flashfloods, the underground water level may rise by as much as 7 m and erode the ceiling of the system of caverns, which can lead to surface subsidence or even sinkholes.

To mitigate the hazards in Valaská, engineering geologists conducted drilling works to lower the level of underground water, in order to lower the threat of creation of new cavern space (hence sinkholes) by erosion due to elevated ground water levels. In 1968 a new sinkhole developed several meters from the spot where the horse had sunk. It was a 4 m wide pit 10 m deep. We were not able to identify its exact location based on historical records or testimonies. New boreholes were executed to further lower the ground water level. These mitigation works, however, had not eliminated the sinkhole hazard in Valaská. The authorities issued an order to tear down houses in the zone of highest threat establishing an exclusion zone lot.

In 2016 geophysical exploration was carried out [30]. In 2019 a new sinkhole developed. Though this one was minor, its occurrence demonstrates that the risk is ongoing due to continuing underground water action. Because of the large volume of the void space of the cave system due to karstification, it was not possible to fill in the void space. Also, the infill would destroy the unique and delicate natural cave system and possibly contaminate the ground water. Instead, following the exploration of 1960-ties, three houses were torn down on the most risk-exposed lot, which was later on protected by fence to prohibit access. The existing sinkholes were roofed by concrete construction components that were further covered by about 2 m of backfill. Also, the surface depressions due to subsidence were backfilled. The debris of the torn-down houses was used as the backfill material.

Sometime prior to 2016, the lot started to be utilized as playground for kids. This stopped after the 2016 exploration, when the playground was moved to a new, stable lot over the road. The sinkhole-threatened lot was turned into an exclusion zone, again.

The geophysical exploration of 2016 [30] comprised dipole electromagnetic profiling (DEMP), microgravimetry, electric resistivity tomography (ERT), georadar (GPR), and refraction seismics. None of the methods (DEMP, ERT, GPR, seismics) has identified or mapped any void space. The

 doi:10.20944/preprints202603.2217.v1

geological interpretation of the ERT profiles, composed into a 3D structural geological model based on resistivity, mapped out in 3D the karstified limestones below the affected area.

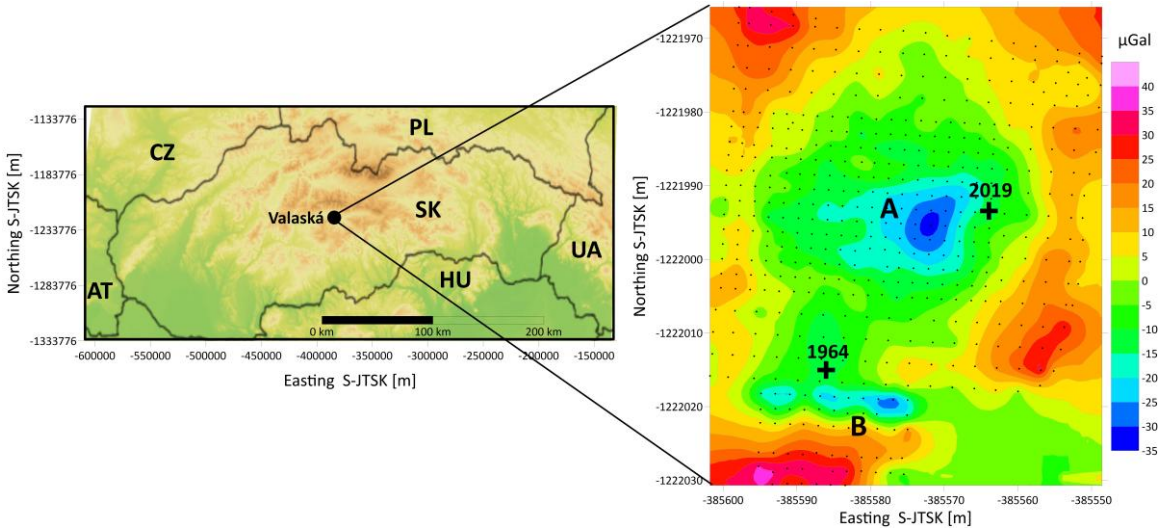

Figure 1. The location of the Valaská village (left) and the residual CBA (RBA) gravity map of the study area (right). The alleged sinkholes of 1964 and 2019 are marked by bold crosses. Data points are marked by dots.

We focus here on the gravity data of the 2016 microgravimetric survey [30] on the emptied lot on which historical sinkholes occurred. It consists of 499 gravity points with spacing 2 m in the central part of the lot and 3 m in the remaining part. The error of observed gravity was estimated at 3 µGal (1 µGal = 10^{-8} m/s^2). Gravity points were precisely geodetically positioned using total station and GNSS observations. Horizontal coordinates (easting and northing) are referenced in the S-JTSK coordinate system. The accuracy of the 3D position is around 2 cm in all three components. Gravity measurements were corrected for the instrument drift. Residual complete Bouguer anomalies (RBA data) were compiled by removing planar trend. The reference density of 2000 kg/m^3 was used in the correction for topographic masses (terrain). The accuracy of the RBA data was estimated at 10 µGal. The RBA map (Figure 1) exhibits a pronounced gravity low of about 35 µGal in the center of the lot (labelled "A") and an alignment of three smaller gravity lows at the southern end of the lot, the middle one (labelled "B") being correlated with the 1964 sinkhole, in which the horse sank. The location of this sinkhole remains somewhat inexact, as it was estimated only by referring to old maps.

We took the gravity data presented in Figure 1 to perform the Growth inversion in order to identify void space (cavities). We use GROWTH-dg software to seek homogenous sources.

3. Growth Inversion for Microgravimetric Cavity Detection

We have already tested the applicability and benefits of the Growth inversion for detection of shallow void space. We have tested the use of Growth in archaeological prospection for microgravimetric detection of crypts or tombs in churches. We managed to successfully detect the known crypts in the St. Nicolas basilica of the Trnava town [26] and in the St. George church of the Svätý Jur town [27] in SW Slovakia. We have also tested the use of Growth for microgravimetric detection of sinkhole hazard in undermined areas at active or abandoned coal mines. At abandoned coal mine of Wolfsberg (Austria), we could successfully detect the top part of a void space that potentially could lead to a sinkhole [26]. At the coal mine in Koš in the Upper Nitra valley of central Slovakia, we were able to successfully detect the back-filled sinkhole [27]. We confirmed an ongoing sinkhole hazard at the abandoned brown coal mine Čáry in the Slovak part of the Vienna Basin and detected the shallow subsurface mining corridors [28]. We also focused on sinkhole hazard in densely populated urban area in a case study in the Pincesor quarters of the Senec town (SW Slovakia) threatened by an extensive complex of mostly unknown underground cellars [27].

 doi:10.20944/preprints202603.2217.v1

In the mentioned case studies, we were searching for cavities already known, meaning we had the "ground truth" to test our approach. This allowed for testing the capabilities of the Growth inversion in recovering the known cavities, indicating the pros and cons of the approach for such purpose. In addition, this facilitated important lessons learnt about the adjustment of the free user-adjustable inversion parameters of the Growth method in those particular case-specific situations and conditions of the near-surface investigations.

We do not present here a complete detailed description of the Growth inversion methodology with its mathematical apparatus and numerical implementation. For that, we refer the reader to [23]. A comprehensive conceptual review of the Growth inversion approach was recently given by Vajda [2026]. Below, we only highlight the key features of this inversion approach mediated by its respective user-adjustable inversion parameters that shape the resulting model.

For our study presented here we use the GROWTH-dg implementation [23] of the inversion approach. The advantage of the GROWTH-dg tool dwells in the option to seek homogenous source bodies of pre-specified density contrasts, which suits well the search for cavities. The density contrast can be pre-set prior to running the inversion. In our Valaská caverns search we use the contrast of -2000 kg/m^3 for void space relative to the sediments or -1670 kg/m^3 for water-filled caverns relative to limestone.

In the Growth inversion approach the volumetric domain below the topographic surface, on which the gravity data are given, is divided into cells, namely right-rectangular prisms, of variable sizes, organized into layers. These are, during the weighted mixed LSA iterative adjustment process, populated step-by-step with the pre-selected density contrast value (both positive and negative), which facilitates the growth of source bodies of the model, represented by aggregations of filled cells. When adequate fit to the gravity data is reached, the process terminates, creating the final model (solution) of the growth process.

The weight between minimizing the data misfit and minimizing the total model mass is governed by the balance factor (λ). The value of λ is pre-set by the user prior to running the inversion and rules the nature and shape of the model, as well as the level of data misfit. The balance factor is the most essential inversion parameter of the Growth approach. Small values of λ produce overfitting models, in which the data noise is translated into model noise in terms of scattered isolated filled prisms or shaggy shapes of source bodies. High values of λ result in over-regularized (over-compacted) models with smaller number of source bodies which attain rounder shapes and may be falsely vertically shifted towards greater depths. We use the adjective "tight-fit" for models that have a misfit r.m.s. close to, or slightly smaller than, the uncertainty (standard deviation) of the input RBA data. Tight-fit models are at the verge of a compact model becoming an overfitting model.

Growth offers an automatically determined default value for λ prior to running the inversion. This value can be over-run by the user. The proper setting of the λ value is assisted by the autocorrelation function displayed on the running screen upon executing Growth. A trial-and-error approach of repeated inversions should be exercised aiming at reaching a nearly null value of autocorrelation for zero distance. Observing the character of the resulting model (not too noisy, not too compacted) throughout this approach is essential. Observing the distribution and size of misfit residuals assists this approach, too.

Another important feature of Growth inversion is the option to co-adjust during the inversion run an offset or planar trend in the input gravity data. In some microgravimetric applications this functionality may turn out to be a must or very beneficial, as we learnt in our previous microgravimetric case studies mentioned above.

Growth offers a useful feature for suppressing or eliminating bad data in the gravity input by means of iterative reweighting controlled by the B (for "blunder") parameter. Such data points can be identified on the running screen as having large misfit residuals. We demonstrate the usefulness of this feature in our Valaská case study below. To run the inversion without iterative reweighting (B>3) is opted for. Smaller B values engage the iterative reweighting. The relationship between the B

 doi:10.20944/preprints202603.2217.v1

value and the strength of the reweighting is case-sensitive and must be tackled by experimenting with the B value in repeated inversion runs.

Another interesting feature of Growth in its GROWTH-dg implementation is the depth weighting functionality controlled by the D (for depth) parameter. When the depth weighting is enabled, the positive (red cells) source bodies are pushed and squeezed towards greater depth (the limit being the bottom boundary of the model domain), while the negative (blue cells) source bodies are pushed and squeezed towards shallower depth (the limit being the topographic surface). From our previous test case studies, we learnt by experience that in case of surficial bodies (their upper boundary coinciding with the topographic surface), strong depth weighting is a must. In other cases, weak or moderate depth weighting may sometime help better recover the true vertical position and depth span of the source bodies.

All the user-adjustable inversion parameters have impact on the character and shape of the solution. This offers the user the opportunity to prepare a whole suite of various solutions with more or less acceptable data misfit and diverse degree of compactness, and then discriminate the individual solutions within the suite based on constraints or external knowledge (if they exist) or simply based on expectations and experience. This is the benefit of the Growth inversion. Also, the user can observe how the Growth solution responds to the changing values of the individual inversion parameters, which may provide hints on the nature of the actual sources.

The variability of the free user-adjustable inversion parameters producing a suite of various Growth models, yet within the limits of reasonable data fit (acceptable misfit), clearly demonstrates the ambiguity of purely gravimetric inversion. This highlights the need for incorporating external constraints or for integration with other geophysical methods, to reduce the ambiguity or to discriminate among the diverse solutions. The variability of the admissible solutions in case of the Valaská data will be presented in Section 4.

Upon completion of the iterative inversion procedure, a final model is obtained. It is graphically displayed on the screen as several horizontal slices (at automatically chosen depths) and several W–E vertical sections (at automatically chosen northings). In addition, two ASCI output files are generated: “Mod.txt” listing the values of the used inversion parameters, and the information about the populated cells; and “Fil.txt” listing the observed, modelled and residual values, including offset/trend. The set of filled cells listed in Mod.txt can be used to import the information into visualization software of third parties to present the model in 3D independently. For that sake we use our own MATLAB script.

Growth was coded to work with UTM coordinates of the input gravity data. If the input gravity is positioned or referenced in different coordinate systems, such as in our case the Slovak national system of S-JTSK, the easting (X) and northing (Y) coordinates must be first transformed into UTM in the input gravity file. Then, for visualization purposes, they can be transformed back to S-JTSK in the output MOD file.

Growth was not originally designed for 3D microgravimetry. When working with microgravity data that have average spacing or grid step of the order of one meter or smaller, Growth might generate cells in the subsurface partition with dimensions below 1 m. This is a problem for Growth, which may result in the output MOD file lacking lines for filled cells with cell size (one cell dimension) smaller than 1 m. This problem can be overcome by using a little trick of upscaling the model domain. The 3D coordinates of data points in the input gravity file are multiplied by an integer n. This results in inflating the dimensions of the cells by n, inflating the volume of the cells by n-cubed, inflating the squared distance between gravity data points and positions of cells by n-squared, and dividing (down-scaling) the density contrast by n. Upon completing the inversion run, prior to visualizing the solution, everything (3D coordinates, cell sizes, and density contrast) is brought back by reverting the upscaling in the MOD file.

 doi:10.20944/preprints202603.2217.v1

4. Growth Model of the Karstic Cavities in the Village of Valaská

We have run Growth inversions on the gravity data presented in Figure 1. Since we are seeking void spaces of a known density contrast (-2000 kg/m^3), we used the GHROWTH-dg software and 1 level of density contrasts, corresponding to homogenous models. To run the Growth inversion, the easting (X) and northing (Y) coordinates of the data points in the input gravity file were first transformed into UTM. To display the Growth solutions (models), the (X, Y) coordinates were transformed back to S-JTSK. We used the upscaling described in Section 3 with $n = 10$. All inversions were run for average cell size of 1.5 m (15 m in the upscaled representation). All inversions in GROWTH-dg were run for homogenous source bodies with density contrast of -2000 kg/m^3, which is the contrast of air relative to the rock medium at the site (-200 kg/m^3 in the upscaling).

All inversions were run with co-adjusted offset and trend, i.e., with planar trend removal. All inversions were run without depth weighting. The blue (negative contrast) source bodies represent void spaces and are the main target of our search. The red (positive contrast) source bodies appear at the circumference of the data area and represent artifacts, due to incompletely removed trend, which in reality may depart from planar. They do not represent real source bodies of geological origin.

GROWTH-dg suggested the default value of balance factor $\lambda = 30$. The model for $\lambda = 30$ turned out to be over-fitting and noisy with tousled (shaggy) source bodies. We therefore increased the balance factor to $\lambda = 60$, which resulted in a tight-fit (residuals: r.m.s. = 7 μGal, max = 21 μGal) compact model presented in Figure 2 (see also Figure S3 in the Supplementary Materials).

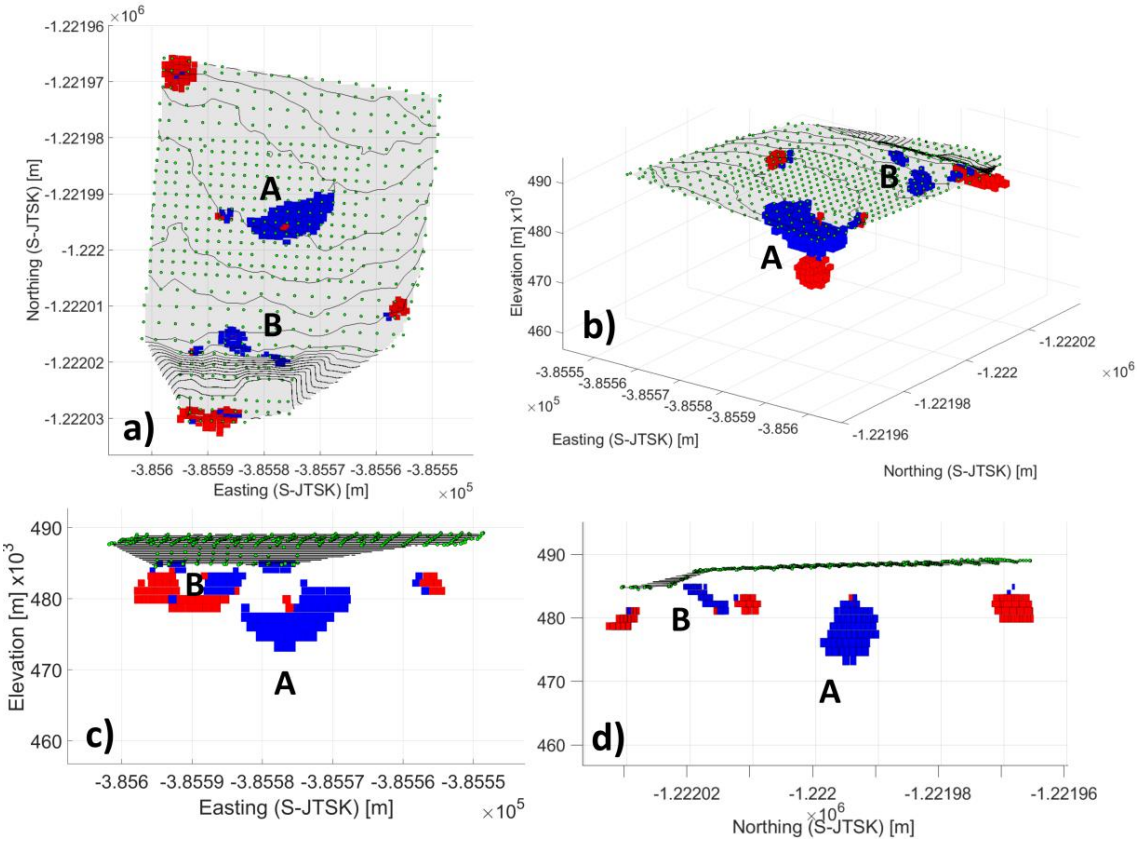

Figure 2. Homogenous (Δρ = -2000 kg/m^3) tight-fit (residuals: r.m.s. = 7 μGal, max = 21 μGal) compact ($\lambda = 60$) Growth model, with removed planar trend, no depth weighting, no iterative residuals re-weighting: (a) top view (azimuth = 0°, elevation = 90°), (b) 3D view from NW (az. = -144°, el. = 20°), (c) lateral view from south (az. = 0°, el. = 0°), (d) lateral view from east (az. = 90°, el. = 0°).

The cavern labelled A, respective to the central gravity low of the 2016 RBA data, spans depths from about 483 m a.s.l. (5 m below surface) to about 474 m a.s.l. (14 m below surface). Viewed from

 doi:10.20944/preprints202603.2217.v1

south or north, it has a sort-of horse-shoe shape. The smaller cavity respective to the 1964 sinkhole, or whatever was leftover of it in 2016 (after partial infill and surficial cover), labelled B, spans vertically from about 2 or 3 m below surface to about 8 m below surface.

In this solution a line of high misfit residuals appears at the edge of the steep terrain slope at the southern end of the data area, lying in the proximity of the gravity low labelled B associated with the 1964 sinkhole (see Figure S3 in the Supplementary Materials). High misfit residuals might indicate "bad input data" (outliers). Therefore, we ran also inversions with enabled iterative residuals reweighting feature with various strengths of the outlier suppression or elimination (various values of parameter B). A tight-fit (residuals: r.m.s. = 6 μGal, max = 9 μGal) compact model (λ = 60) with co-adjusted (removed) planar trend, no depth weighting, and a very strong residuals reweighting (B = 1.3) is presented in Figure 3 (see also Figure S4 in the Supplementary Materials). This very strong residuals reweighting resulted in eliminating the cavern B from the model. It also eliminated the red (positive contrast) source bodies at the circumference of the data area. When medium or weak residuals reweighting was applied (not presented here), the models contained also the cavern B, but it was smaller than when applying no residuals reweighting.

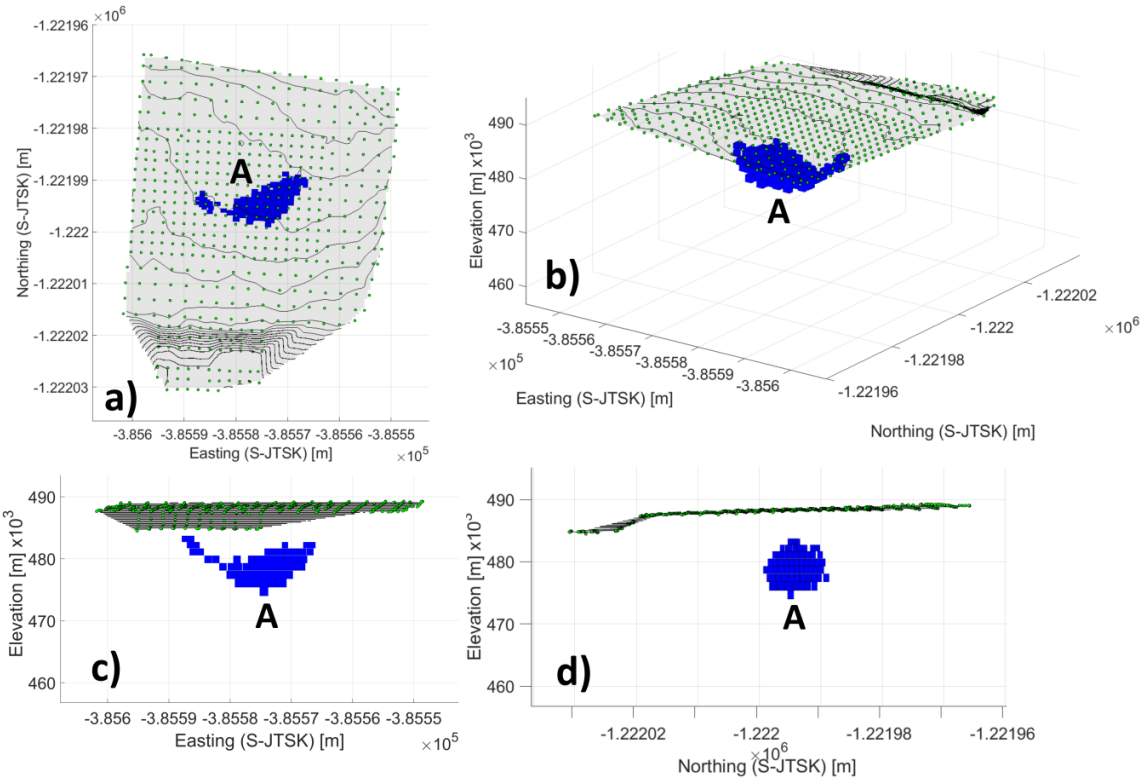

Figure 3. Homogenous ($\Delta\rho$ = -2000 kg/m^3) tight-fit (residuals: r.m.s. = 6 μGal, max = 9 μGal) compact (λ = 60) Growth model, with removed planar trend, no depth weighting, and very strong iterative residuals re-weighting (B = 1.3): (a) top view, (b) 3D view from NW (az. = -144°, el. = 20°), (c) lateral view from south (az. = 0°, el. = 0°), (d) lateral view from east (az. = 90°, el. = 0°).

Even a strong residuals reweighting has not completely eliminated the worst misfit residuals at the southern end of the lot (see Figure S4 in the Supplementary Materials). These data points are close to a terrain edge (steep slope). This brought up suspicion that the poor quality of the data here may be related to the terrain correction in the CBA data. Out of curiosity, we compiled a new residual CBA dataset with terrain correction based on the most recent LiDAR-derived digital terrain model (DTM) that was not available in 2016. The new residual CBA (RBA) map compared to that of 2016 is shown in Figure 4. It is clear that the quality of the DTM affects the RBA map in the vicinity of the steep slope (terrain edge) at the southern end of the lot, and consequently the character of cavern B identified by the inversion.

 doi:10.20944/preprints202603.2217.v1

We ran the Growth inversion on this new RBA dataset with the same inversion parameters as those of the compact homogenous model presented in Figure 2. The resulting model (with misfit: r.m.s. = 6 μGal, max = 20 μGal) is presented in Figure 5 (see also Figure S11 in the Supplementary Materials). This solution is very similar to the solution based on 2016 RBA data with moderate residuals reweighting (not presented here). That means that the partial inadequacy of the 2016 RBA data at the edge of the steep slope can be suppressed or counter-acted by the moderate residuals reweighting feature of Growth.

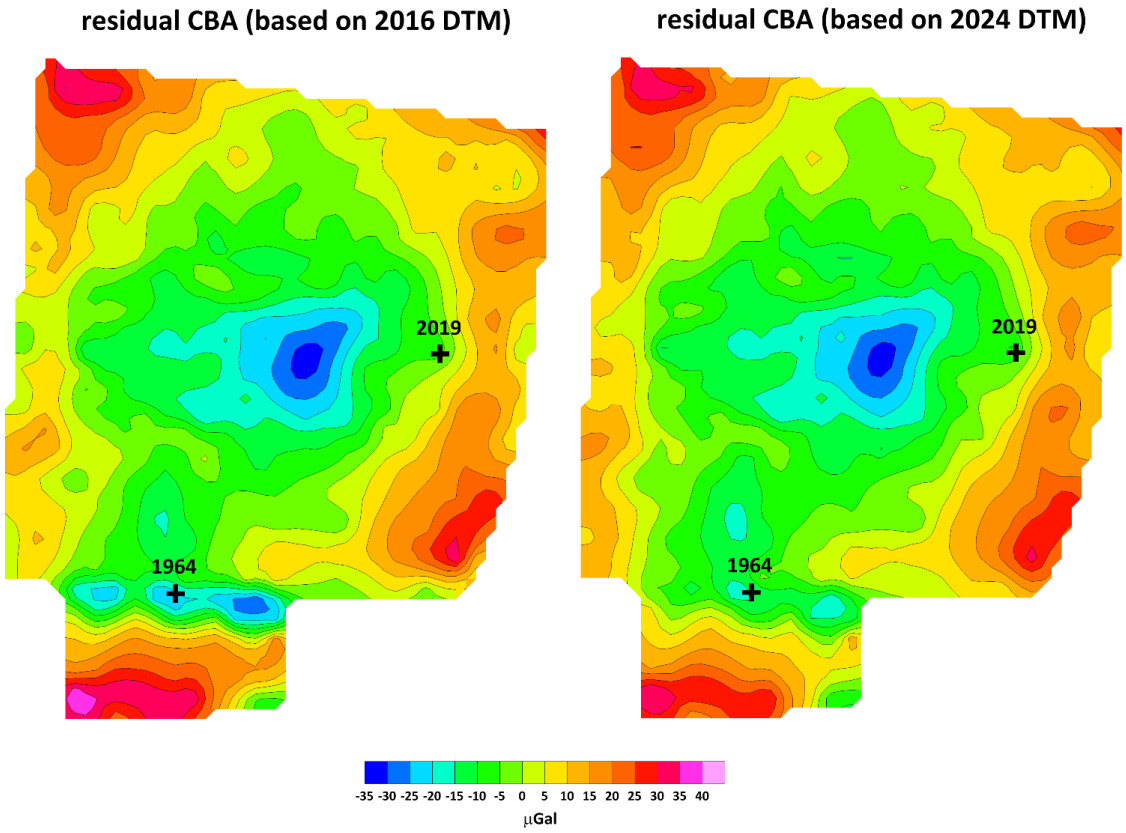

Figure 4. The impact of the quality (accuracy and resolution) of the DTM (old on left, new on right) used to compile the RBA data is seen at the southern data area end, close to the steep terrain slope.

Even the newly compiled residual CBA data with the use of the 2024-LiDAR-based DTM are not completely free of the effect of the steep slope (see Figure S11 in the Supplementary Materials). Therefore, we run another inversion with engaged residuals reweighting even on the data based on the 2024 DTM. In Figure 6 (see also Figure S12 in the Supplementary Materials), we present a similar Growth model to that of Figure 5, with the same inversion parameters, this time with engaged fairly strong iterative reweighting of residuals (B = 1.6).

The Growth inversion solutions for the Valaská 2016 CBA data give us a pretty much consistent picture of the presence of cave space, manifested by caverns A and B, and associated sinkhole hazard (respective to year 2016) on the lot (currently exclusion zone) in the Valaská village. The cavern respective to the central and most pronounced gravity low (labelled A) is the most significant cavity revealed by microgravimetry. Due to the proximity of its upper boundary to the surface (5 to 4 m), we conclude that this cavern poses a sinkhole development threat. The cavern labelled B is related to the 1964 sinkhole. That the strongly karstified area under the lot is still prone to sinkhole development was confirmed by the occurrence of a small sinkhole in 2019.

 doi:10.20944/preprints202603.2217.v1

5. Discussion

Purely gravimetric interpretation is very ambiguous. The ambiguity is illustrated also by the variability of Growth solutions, which are admissible in terms of data fit, for the variable values of the individual Growth inversion parameters. In addition, the interpreted local gravity anomaly, which is the residual CBA anomaly, is relative in terms of offset. Consequently, the gravimetric interpretation must be assisted or constrained by additional geophysical methods or additional independent cognition. We therefore interpret our obtained inversion models in the context of the findings of the exploration reported by Kubíny [32] and in [30].

Based on geological, geomorphological and speleological works, Kubíny has assumed the presence of underground ponds and caverns even before 1956. Subsequent speleological (including scuba-diving) exploration [31] confirmed the cave space in the Valaská subsurface. In the sinkhole accident of 21 Sept., 1964, the horse had sunk into a roughly 1 m narrow 9 m deep karst chimney. Below this 9 m deep sinkhole a cavity was found to the side of it, another 20 m deep, which was filled with water and explored by divers. The bottom part of this cavern was connected with a fast-flowing underground river (see Supplementary Materials, Figure S5). In autumn of 1968 and in February of 1969, two new sinkholes appeared near that of 1964. The preliminary exploration has confirmed a high-degree karstification of limestones below the Valaská village in the forefield of the Tajch spring, and the existence of deep and extensive underground water pools [32].

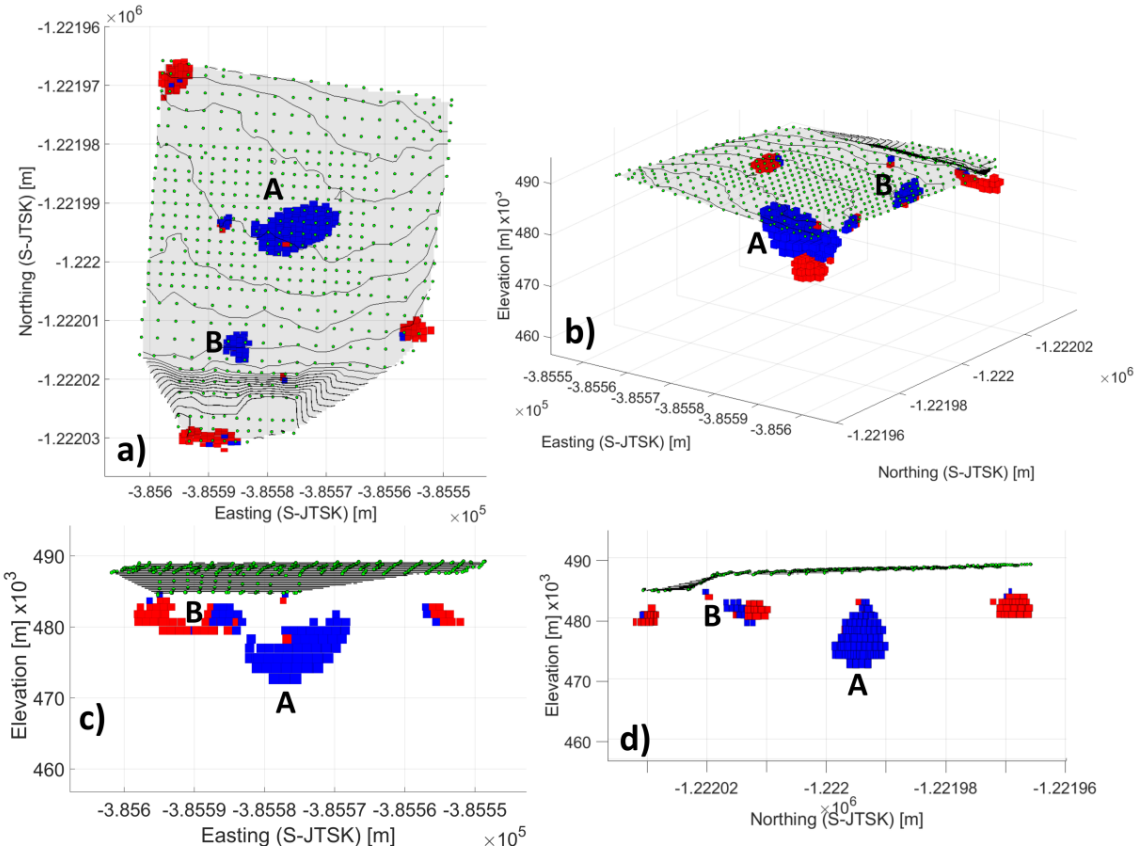

Figure 5. Homogenous ($\Delta\varrho$ = -2000 kg/m^3) tight fit (residuals: r.m.s. = 6 μGal, max = 20 μGal) compact (λ = 60) Growth model with removed planar trend, no depth weighting, and no residuals re-weighting for the new residual CBA dataset compiled with terrain correction based on the most recent (2024) LiDAR-derived DTM: (a) top view, (b) 3D view from NW (az. = -144°, el. = 20°), (c) lateral view from south (az. = 0°, el. = 0°), (d) lateral view from east (az. = 90°, el. = 0°).

These underground spaces are associated with NNE–SSW trending tectonic fractures to which the main underground river of Valaská is linked. Along this system other caverns and galleries are

 doi:10.20944/preprints202603.2217.v1

expected, due to pressure erosion by water, that are filled by water up to the hydrostatic level. To them belong also karst cavities detected by boreholes V2, V3, ŠV2 (see Figures S5–S10 in the Supplementary Materials). Borehole V2 went through the intensively karstified limestones, partially filled with lime, from 8.3 to 18 m depth. Karst cavities in Valaská, associated with the known sinkholes, are up to 30 m deep and up to 10 m wide [32].

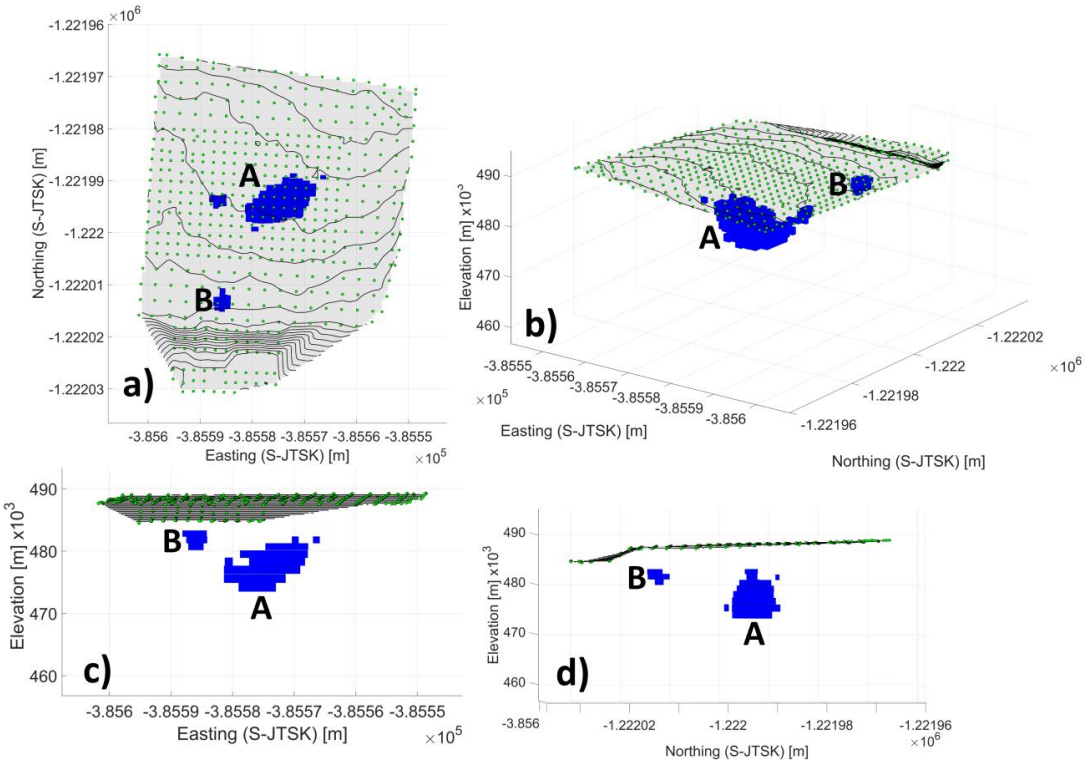

Figure 6. Homogenous ($\Delta\varrho$ = -2000 kg/m^3) tight fit (residuals: r.m.s. = 6 μGal, max = 10 μGal) compact (λ = 60) Growth model with removed planar trend, no depth weighting, and engaged residuals re-weighting (B = 1.6) for the new residual CBA dataset compiled with the 2024-LiDAR-derived DTM: (a) top view, (b) 3D view from NW (az. = -144°, el. = 20°), (c) lateral view from south, (d) lateral view from east).

The report of Kubíny [32] concludes with recommendations for mitigating the sinkhole hazard. The degree of karstification (one third of the limestone volume estimated as cavities) in the highest threat zone (zone I in the map of Figure S6 in the Supplementary Materials) is such that the area cannot be made safe by filling-in the caverns (infill material estimated at 70 million m^3). Instead, Kubíny proposes to make the cave system with underground ponds accessible to public, with the entry built at the little shaft ŠV-1 and the exit at the sinkhole-1 (see the map in the Supplementary Materials).

In order to identify the sinkhole hazard at the studied lot in the Valaská village, and to detect the void (cave) space underneath the lot, respective to the situation in 2016, as reflected by the microgravity data collected in 2016, we inverted the gravity data with the GROWTH-dg software. First, we experimented, using a trial-and-error process, with the balance factor value (λ). We found out that λ = 60 produces tight-fit yet compact solutions.

In the obtained solutions we observed the presence of data points with poor data fit (large misfit residuals) lined-up at the edge of the steep terrain slope at the southern end of the lot. These bad data points called for the engagement of iterative reweighting. Strong iterative reweighting eliminated the contribution of these points into the solution. This resulted in eliminating the three small void spaces at the southern end of the lot from the solution. Moderate reweighting weakened the contribution of these data points, which resulted in eliminating the two small void spaces surrounding the space

 doi:10.20944/preprints202603.2217.v1

labelled B at the southern end of the lot from the solution and decreasing the size (volume) of the cavern labelled B, which is associated with the 1964 sinkhole.

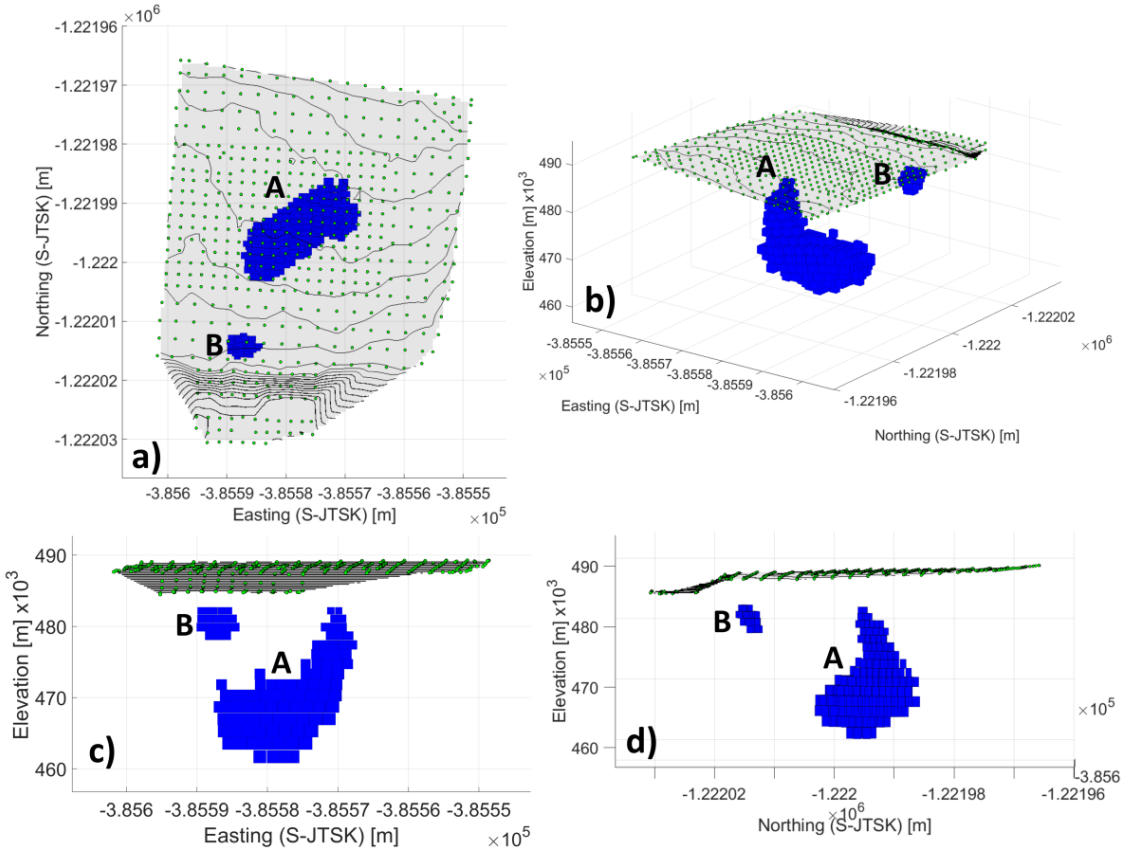

Figure 7. Homogenous ($\Delta\varrho$ = -2000 kg/m^3) tight-fit (residuals: r.m.s. = 6 μGal, max = 11 μGal) compact (λ = 60) Growth model with no trend removal, no depth weighting, weak residuals reweighting (B = 2.2) for the 2016 RBA data with arbitrarily added offset of -20 μGal: (a) top view, (b) 3D view from NW (az. = -144°, el. = 20°), (c) lateral view from south, (d) lateral view from east).

Since the bad data points line-up in the proximity of the terrain slope edge, this gave rise to the suspicion that they might be a consequence of a partial failure of the topographic (terrain) correction in the CBA data compilation at this place due to low resolution or accuracy of the digital terrain model (DTM), available in 2016, at this slope edge. Thus, we performed a methodological experiment, compiling a new residual CBA data set based on terrain correction computed with a more recent (2024) LiDAR-derived DTM of higher quality, which however was not available in 2016. Then we inverted the new RBA data with the outcome similar to using moderate iterative reweighting on the 2016 dataset, as discussed in Section 4. Both Growth solutions indicate the presence of the cavern (labelled B) associated with the 1964 sinkhole.

Since the residual CBA data are relative in terms of offset, we tested also adding a negative 20 μGal offset (arbitrarily chosen value) to the residual CBA data. Upon inversion of such data, we obtained larger and deeper caverns A and B, cf. the Growth model of Figure 7 (see also Figure S13 in the Supplementary Materials). This illustrates another level of ambiguity of purely gravimetric interpretation.

For additional depth estimation to the source of the main local gravity low labelled "A", we used the 3D Euler deconvolution method [33] with incorporated regularized derivatives [34]. Using a predefined structural index value of 2 (respective to a spherical source in gravimetry), we obtained a cluster of solutions at the depth of approximately 6 m (see Figure S14 in the Supplementary Materials).

 doi:10.20944/preprints202603.2217.v1

We can summarize the results of our Growth inversion as follows. We have detected the presence of the top part of the secured (covered-up) cavern adjunct to the 1964 sinkhole. We have detected the presence of a larger cavern related to the central most pronounced gravity low. We speculate that this cavern is associated with the 1968 and 1969 sinkholes, though their exact location cannot be identified or validated. Our speculation is supported by the fact that the 1968 sinkhole was considerably bigger (4 by 10 m) than the 1964 sinkhole (1 by 9 m), while likewise our detected cavern A compares to cavern B. Even as for cavern A we assume that we are catching only its top part, not the whole cavern.

The density contrast -2000 kg/m^3 used in our inversion is that of the air against the density of quaternary sediments. This fits well the situation of the empty top parts of the caverns (to ca. 7 m below surface). Deeper down the situation is characterized by water filled caverns in limestone background, yielding a density contrast of -1670 kg/m^3. Therefore, we ran the inversions also with this contrast (not presented here). The change of contrast did not have much effect on the character of the solutions. The detected caverns were slightly larger, but of similar shapes and depth spans.

6. Conclusions

The whole spectrum of diverse admissible Growth models for the Valaská residual CBA microgravity data yielded pretty much the same information about the existence of cavern labelled "A" related to the main gravity low in the center of the lot. We assume we have detected only the top part of this cavern. Its top boundary was detected at 5 to 4 m below surface, which is already cut through the interface (ceiling) of the loess clay, critical for sinkhole development. We hypothesize that this cavern is associated with the 1968 sinkhole and perhaps also the 1969 sinkhole. Such hypothesis cannot be verified, as it is not possible to locate the two sinkholes based on existing records or testimonies.

The spectrum of admissible Growth models for the Valaská residual CBA (RBA) microgravity data revealed also the existence of the top part of cavity labelled B, most likely associated with the 1964 sinkhole of the horse accident, as the cavern northward to the side of the sinkhole (cf. Figure S5 in the Supplementary Materials).

The Valaská case study has demonstrated that the Growth inversion approach in its GROWTH-dg implementation is a versatile tool for microgravimetric investigations in karst areas. It is suitable and useful for shallow cave space detection and can assist in sinkhole hazard mitigation. By revisiting the gravity data in Valaská we have shown by means of the Growth inversion of microgravity data that the sinkhole hazard at the lot is ongoing. We recommend that the microgravimetric methodological approach presented here be used in other karst areas to detect new shallow cave space or assist in sinkhole hazard evaluation.

Supplementary Materials: The following supporting information can be downloaded at the website of this paper posted on Preprints.org.

Author Contributions: Conceptualization, J.B., P.V., and P.Z.; methodology, J.B., P.V., and J.F.; software, J.B., P.V., and J.F.; validation, P.Z., R.Pa., R.Pu., and J.P.; formal analysis, P.Z. and J.F.; investigation, P.V., P.Z. and R.Pu.; resources, P.V.; data curation, P.Z., J.P. and J.B; writing—original draft preparation, P.V.; writing—review and editing, P.Z. and J.F.; visualization, P.Z. and J.B.; su-pervision, P.V.; project administration, P.V.; funding acquisition, P.V., J.B., P.Z., R.P., and J.F. All authors have read and agreed to the published version of the manuscript.

Funding: J.F. and J.B. were supported by Spanish Agencia Estatal de Investigación (10.13039/501100011033) grant G2HOTSPOTS (PID2021-122142OB-I00) and RADARQUIFER (MITECO 20233TE014). J.B. was supported also by the DoktoGrant grant system of the Slovak Academy of Sciences through the project No. APP0652. This work was partially supported also by the Slovak Research and Development Agency under the contract (project) No. APVV-19-0150 (acronym ALCABA), and by the VEGA grant agency under projects No. 2/0002/23 and No. 1/0587/24.

 doi:10.20944/preprints202603.2217.v1

Data Availability Statement: The GROWTH-dg software (including source code) and user manual are free, available for download from the websites: http://gegrage.ucm.es/en/software-en/or https://github.com/josefern/Growth-dg. Alternatively, the executable can be obtained by contacting the first author. The residual CBA data are available upon request.

Acknowledgments: No AI tools were used in this work or to prepare the manuscript.

Conflicts of Interest: The authors declare no conflicts of interest. The funders had no role in the design of the study; in the collection, analyses, or interpretation of data; in the writing of the manuscript; or in the decision to publish the results.

References

1. Omnes, G. High accuracy gravity applied to the detection of karstic cavities, In: *Karst hydrogeology*, Tolson, J.S.; Doyle, F.L. (Eds.), UAH Press, **1977**, vol. 12, 273–284
2. Butler, D.K. Microgravimetric and gravity gradient techniques for detection of subsurface cavities. *Geophysics* **1984**, 49, 1084–1096, doi:10.1190/1.1441723
3. Bishop, I.; Styles, P.; Emsley, S.J.; Ferguson, N.S. The detection of cavities using the microgravity technique: case histories from mining and karstic environments, In: *Modern Geophysics in Engineering Geology*, McCann, D.M.; Eddleston, M.; Fenning, P.J.; Reeves, G.M. (Eds), **1997**, Geological Society Engineering Geology Special Publication No. 12, 153–166
4. Mochales, T.; Casas, A.M.; Pueyo, E.L.; Pueyo, O.; Román, M.T.; Pocoví, A.; Soriano, M.A.; Ansón, D. Detection of underground cavities by combining gravity, magnetic and ground penetrating radar survey: A case study from the Zaragoza area, NE Spain. *Environmental Geology* **2008**, 53, 1067–1077, doi:10.1007/s00254-007-0733-7
5. Gambetta, M.; Armadillo, E.; Carmisciano, C.; Stefanelli, P.; Cocchi, L.; Tontini, F.C. Determining geophysical properties of a near-surface cave through integrated microgravity vertical gradient and electrical resistivity tomography measurements. *Journal of Cave and Karst Studies*, **2011**, v. 73, no. 1, 11–15, doi:10.4311/jcks2009ex0091
6. Putiška, R.; Kušnirák, D.; Dostál, I.; Lačný, A.; Mojzeš, A.; Hók, J.; Pašteka, R.; Krajňák, M.; Bošanský, M. Integrated Geophysical and Geological Investigations of Karst Structures in Komberek, Slovakia. *Journal of Cave and Karst Studies*, **2014**, v. 76, no. 3, 155–163, https://dx.doi.org/10.4311/2013ES0112
7. Braitenberg, C.; Sampietro D.; Pivetta, T., Zuliani, D.; Barbagallo, A.; Fabris, P.; Rossi, L.; Fabbri, J.; Mansi, A.H., Gravity for Detecting Caves: Airborne and Terrestrial Simulations Based on a Comprehensive Karstic Cave Benchmark. *Pure and Applied Geophysics*, **2015**, 173, 1243–1264, https://doi.org/10.1007/s00024-015-1182-y
8. Land, L; Rinehart, A. Geophysical surveys of a potentially extensive cave system, Guadalupe Mountains, New Mexico, USA. *Journal of Cave and Karst Studies*, **2018**, vol. 80, no. 3, 109–120, doi: 10.4311/2017ES0108
9. El-Qady, G.; Hafez, M.; Abdalla, M.A.; Ushijima, K. Imaging subsurface cavities using geoelectric tomography and ground-penetrating radar. *Journal of Caves and Karst Studies*, **2005**, vol. 67, no. 3, 174–181
10. Cardarelli, E.; Cercato, M.; Cerreto, A.; Di Filippo, G. Electrical resistivity and seismic refraction tomography to detect buried cavities: *Geophysical Prospecting*, **2010**, 58, 685–695, doi:10.1111/j.1365-2478.2009.00854.x
11. Andrej, M.; Uroš, S., Electrical resistivity imaging of cave Divaška jama, Slovenia. *Journal of Cave and Karst Studies*, **2012**, vol. 74, no. 3, 235–242, doi:10.4311/2010ES0138R1
12. Putiška, R.; Nikolaj, M.; Dostál, I.; Kušnirák, D. Determination of cavities using electrical resistivity tomography: *Contributions to Geophysics and Geodesy*, **2012**, vol. 42, no. 2, 201–211, https://doi.org/10.2478/v10126-012-0018-3
13. McCrackin, Ch.W.; Kiflu, H.G.; Kruse, S.E.; van Beynen, Ph.E.; Polk, J.S.; Miller, B. 3D resistivity survey over mapped caves in eogenetic karst terrane, west-central Florida, USA. *Journal of Cave and Karst Studies*, **2022**, vol. 84, no. 1, 1–13. doi:10.4311/2017ES0125

 doi:10.20944/preprints202603.2217.v1

14. Di Fiore, V.; Angelino, A.; Passaro, S.; Bonanno, A. High resolution seismic reflection methods to detect near surface tuff-cavities: a case study in the Neapolitan area, Italy. *Journal of Cave and Karst Studies*, **2013**, vol. 75, no. 1, 51–59, doi: 10.4311/2011ES0248
15. Dobecki, T.L.; Upchurch, S.B. Geophysical applications to detect sinkholes and ground subsidence. *The Leading Edge*, **2006**, 25, 336–341, doi:10.1190/1.2184102
16. Kaufmann, G.; Romanov, D.; Nielbock, R. Cave detection using multiple geophysical methods: Unicorn cave, Harz Mountains, Germany. *Geophysics*, **2011**, vol. 76, no. 3, B71–B77, doi:10.1190/1.3560245
17. Zahorec, P.; Marušiak, I.; Mikuška, J.; Pašteka, R.; Papčo, J. Numerical Calculation of Terrain Correction Within the Bouguer Anomaly Evaluation (Program Toposk), In: *Understanding the Bouguer Anomaly: A gravimetry Puzzle*. Pašteka, R.; Mikuška, J.; Meurers, B. (eds). **2017**, 79–92. Elsevier, ISBN 978–0-12–812913–5
18. Camacho, A.G.; Montesinos, F.G.; Vieira, R. A 3-D gravity inversion tool based on exploration of model possibilities. *Computers and Geosciences*. **2002**, 28, 191–204, https://doi.org/10.1016/S0098-3004(01)00039-5
19. Camacho, A.G.; Fernández, J.; Gottsmann, J. A new gravity inversion method for multiple sub-horizontal discontinuity interfaces and shallow basins. *Journal of Geophysical Research*, **2011**, vol. 116, B02413, https://doi.org/10.1029/2010JB008023
20. Camacho, A.G.; Gottsmann, J.; Fernández, J. The 3-D gravity inversion package GROWTH2.0 and its application to Tenerife Island, Spain. *Computers and Geosciences*. **2011**, 37, 621–633, https://doi.org/10.1016/j.cageo.2010.12.003
21. Camacho, A.G.; Prieto, J.F.; Aparicio, A.; Ancochea, E.; Fernández, J. Upgraded GROWTH 3.0 software for structural gravity inversion and application to El Hierro (Canary Islands). *Computers and Geosciences*. **2021**, vol. 150, 104720. https://doi.org/10.1016/j.cageo.2021.104720
22. Camacho, A.G.; Vajda, P.; Fernández, J. GROWTH-23: An integrated code for inversion of complete Bouguer gravity anomaly or temporal gravity changes. *Computers and Geosciences*, **2024**, vol. 182, 105495, https://doi.org/10.1016/j.cageo.2023.105495
23. Camacho, A.G.; Vajda, P.; Miller, C.A.; Fernández, J. A free-geometry geodynamic modelling of surface gravity changes using GROWTH-dg software. *Scientific Reports*. **2021**, vol. 11, 23442. https://doi.org/10.1038/s41598-021-02769-z
24. Vajda, P.; Camacho, A.G.; Fernández, J. Benefits and limitations of the Growth inversion approach in volcano gravimetry demonstrated on the revisited Tenerife 2004–2005 unrest. *Surveys in Geophysics* **2023**, 44, 527–554. https://doi.org/10.1007/s10712-022-09738-9
25. Camacho, A.G.; Vieira, R.; Montesinos, F.G.; Cuéllar, V. A gravimetric 3D Global inversion for cavity detection. *Geophysical Prospecting*, **1994**, 42, 113–130. https://doi.org/10.1111/j.1365-2478.1994.tb00201.x
26. Vajda P.; Bódi, J.; Camacho, A.G.; Fernández, J.; Pašteka, R.; Zahorec, P.; Papčo, J. Gravimetric inversion based on model exploration with growing source bodies (Growth) in diverse earth science disciplines. *AIMS Mathematics*, **2024**, vol. 9, no. 5, 11735–11761. doi: 10.3934/math.2024575
27. Bódi J.; Vajda, P.; Pašteka, R.; Pánisová, J.; Papčo, J.; Zahorec, P.; Fernández, J. Applicability of Growth inversion in microgravimetry for archeological prospection and sinkhole hazard detection: Jur, Koš and Senec case studies. *Journal of Applied Geophysics* **2025**, Vol. 238, 105718, https://doi.org/10.1016/j.jappgeo.2025.105718
28. Bódi J.; Vajda, P.; Zahorec, P.; Pašteka, R.; Papčo, J.; Putiška, R.; Brixová, B.; Fernández, J. Gravimetric detection of sinkhole hazard at abandoned coal mine Čáry (Slovakia) using Growth inversion—preliminary results. *Contributions to Geophysics and Geodesy*, **2026**, vol. 56, no. 1, 65–83 (in press)
29. Múka, Ľ., 2023, Prepadové územie vo Valaskej (in Slovak), Sinkhole area in Valaská, Speleo Brezno web portal: https://osbr.sss.sk/prepadove-uzemie-vo-valaskej/(accessed 28 Feb., 2025)
30. Putiška, R. Geofyzikálny prieskum a posúdenie stability potencionálneho prepadového územia v obci Valaská (in Slovak). Geophysical exploration and stability assessment of the potentially sinkhole-prone area in the Valaská village, **2016**, AEG Ltd. Report
31. Kalaš, L. Podzemné priestory v obci Valaská (in Slovak). Underground space in village Valaská, **1965**, final report

 doi:10.20944/preprints202603.2217.v1

32. Kubíny, D. Správa o geologických a speleologických pomeroch prepadového územia vo Valaskej pri Brezne. Slovenský kras XII (in Slovak) Report on geological and speleological conditions in the sinkhole area of Valaská near Brezno. **1975**, Slovak Karst XII
33. Reid A.B.; Allsop J.M.; Granser H.; Millet A.J.; Somerton I.W. Magnetic interpretation in three dimensions using Euler deconvolution. *Geophysics* **1990**, 55, 80–91, https://doi.org/10.1190/1.1442774
34. Pašteka R.; Richter F.P.; Karcol R.; Brazda K.; Hajach M. Regularized derivatives of potential fields and their role in semi-automated interpretation methods. *Geophysical Prospecting* **2009**, 57, 507–516, https://doi.org/10.1111/j.1365-2478.2008.00780.x